Droplet Deposition Pattern Affected by Different Heating Directions

Zeyu Liu[1], Yuying Yan[1,2*], Xin Wang[1], Xinyong Chen[3]

1. *Fluids & Thermal Engineering Research Group, Faculty of Engineering, University of Nottingham, Nottingham, NG7 2RD, UK*

2. *Fluids & Thermal Engineering Research Centre, University of Nottingham, Ningbo 315100, China*

3. *School of Pharmacy, Faculty of Science, University of Nottingham, Nottingham, NG7 2RD, UK*

Abstract

The coffee ring effect commonly exists in droplet deposition patterns, which fundamentally affects scientific research and industrial applications, like pharmaceutical purification, salt manufacturing, etc. Some researchers have tried different solutions to control the distributions of droplet deposition patterns, but most control deposits by adjusting droplet characteristics. In this work, droplet deposition patterns with different wettability are investigated by both localized and substrate heating. A whole process of droplet evaporation is recorded. The droplet generally evaporates from constant contact radius (CCR) mode to constant contact angle (CCA) mode, and CCR stage occupies the most of time. Experimental results show that, without any chemicals, laser induced local heating transitions particle deposition patterns from ring-like structure to dot-like patterns on a hydrophilic surface, driving most saline solvent to the center. Meanwhile, a hydrophobic surface is also investigated showing that the particles tend to assemble at the central area, but the pattern is slightly different compared to that on hydrophilic surface. In addition, physical mechanisms of local heating and heating from substrate are also explored in the present study.

Keywords: saline, droplet, deposition pattern, local heating.

***Corresponding author:** Yuying Yan
E-mail: yuying.yan@nottingham.ac.uk

1 Introduction

Coffee ring effect is a stain pattern deposited by non-volatile solute of liquid after evaporation, which is named due to the ring-like deposition after complete evaporation. However, coffee ring effect is not welcomed in many industrial applications, such as pharmaceutical purification[1, 2], salt manufacturing[3, 4], inkjet printing[5-7], DNA microarrays[8-10], nanotechnology[11-15] and so on. Therefore, it has encouraged many researchers to explore effective methods to control the distribution of the drying of suspension droplets actively, and study on the mechanism of different deposition patterns.

Droplet evaporation can be typically classified in two modes, constant contact radius (CCR) mode and constant contact angle (CCA) mode[16]. The interests in droplet deposition pattern research was inspired after ring stain was firstly proposed and analysed by Deegan[17]. Heated from the substrate uniformly, the evaporation flux at the edge is evidently higher than other positions, forcing particles inside to transport from central area toward to periphery for compensating the solvent loss. Eventually, evaporation flow carries the central particles to the edge, resulting in most solute deposited at the edge, forming a ring-like structure.

In order to suppress the formation of deposits, scholars have made many efforts on controlling the distribution of deposition patterns. Mainak et al.[18] experimentally suppress coffee ring effect under volatile condition, which is able to assist Marangoni flow. Dan Soltman et al.[5] investigated contributions of droplet spacing and temperature on droplet deposition pattern. In their research, they found an optimized condition to control the size of pattern. Alexandros Askounis et al.[19] studied on biodrop deposition and found that morphology of biodrop can change the ratio of CCR and CCA in the process of evaporation. In addition, Chen et al.[20] experimentally showed the onset time for CCR-CCA transition and the critical base size at the Cassie-Wenzel transition exhibit remarkable dependence on the surface roughness. And also, many researchers [17, 21-24]

found that Marangoni flow and capillary flow are two significant factor influencing deposition pattern and tried to subject formation through balancing them.

On the other hand, droplet evaporation is a ubiquitous phenomenon that can be observed in nature, such as rain drops falling on lotus leaf, dew drop on the windshield. In the evaporation process, the surface can be self-cleaned[25, 26] without water stain due to its hydrophobic property. Moreover, in the evaporation process, liquid phase water absorbs heat from surrounding and change into vapor phase[27], which also affected the distribution of sediment in nature. Therefore, it is inspired from the nature that the study of wettability on the distribution of deposit can be an efficient method to control droplet deposition pattern without additional chemicals.

Most scholars are trying to control droplet deposition patterns with chemicals. However, many applications cannot change the characters of solutions in order to control the distribution of deposition patterns. Inspired by droplet focusing on collecting solar energy, if enough energy is collected in a local area, uneven heating will affect the flow motion in the droplet due to the temperature gradients. This work aims to explore an effective method to control the distribution droplet deposition patterns without chemicals. The deposition patterns of saline solution with different wettability are experimentally investigated by heating from apex and substrate respectively. Meanwhile, the whole process of droplet evaporation is recorded. Physical mechanism of such phenomenon in different conditions is also analysed.

2 Fabrication of materials for coating on the substrate

In this work, saline droplet, as a soluble solution, can disperse solutes better than the mixture, but is not affected by gravity and dispersibility. Therefore, it can better understand the effect of local heating on the distribution of the deposition patterns by the saline solution. The saline droplets are prepared by dissolving sodium chloride powders (NaCl, >99%) into deionized water.

The solutions were first stirred for half an hour. There are two batches with the saline concentration of 2.0%. Substrate heating and local heating are both conducted on hydrophobic and hydrophilic surface respectively.

The hydrophobic material coated on the substrate in the experiment is a combination of nanoparticles and functional materials in solution[28]. Silica (SiO_2) nanoparticles (fumed powder) with average size 7nm and poly dimethyl siloxane (PDMS) solution (Molecular weight 95000, Fluka) were purchased from Sigma Aldrich. Firstly, PDMS is dissolved in the white spirit solvents, forming the solutions with a concentration of 6 wt.%, prior to adding nanoparticles. The SiO_2 nanoparticles with 7nm are then dispersed into solution with concentration of 0.5, 1.0, and 2.0% w/v respectively. Among them, 2.0%w/v exhibits better hydrophobic property than other concentrations.

For hydrophilic surface, magnetic nanofluids are coated on the substrate, which are synthesised by two-step method. $FeCl_3 \cdot 6H_2O$ and $FeCl_2 \cdot 4H_2O$ are firstly dissolved in deionized water. After removing oxygen through nitrogen for 15min, ammonium hydroxide is added to solution under vigorous stirring with temperature of 60°C. With aid of ultrasonic treatment, precipitate collected is then modified by citric acid, and finally disperses into base liquid[29].

PDMS-SiO_2 and magnetic nanofluids are both deposited onto the substrate through air brush system. The coated substrates are dried in an oven with 40°C for 2 hours. Subsequently, the treated substrates are kept at ambient temperature for 2 days before experiments. As shown in Fig.1 and Fig.2, the contact angle of hydrophobic surface is 111.91°, and the contact angle of hydrophilic surface is 25.96°.

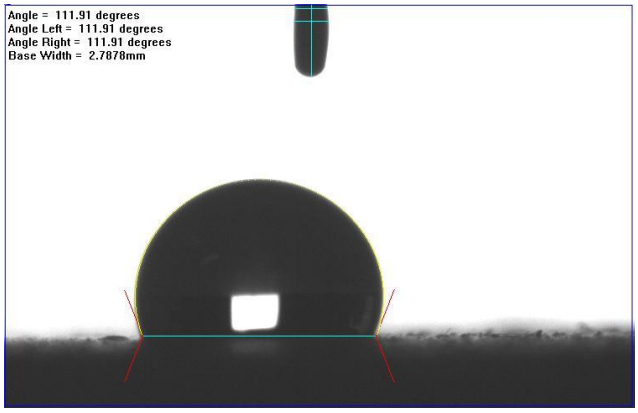

Fig.1 Contact angle of hydrophobic surface coated by PDMS-SiO2.

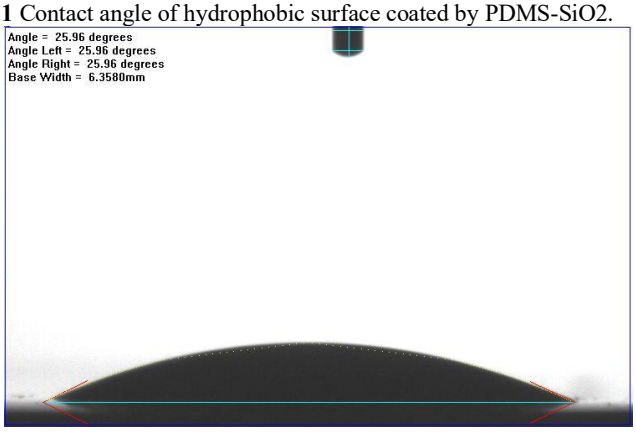

Fig.2 Contact angle of hydrophilic surface coated by magnetic nanofluids.

3 Experimental set-up

The experimental set-up is as shown is Fig.3 The saline drop has strong spectral absorption performance when the wavelength of the spectrum is in the infrared region, which is beyond 780nm. In order to supply heat source from different directions, we applied a 500mW laser system with the wavelength of 1.2μm, which means that saline solution is able to absorb heat from the induced laser. Meanwhile, it is located from the apex of saline droplet with the concentration of 2wt.%. In addition, the volume of saline is 2μL, which is controlled by pipette for each test. A phantom v640 CCD camera is used to record the whole process of evaporating saline droplet. LEDs array illuminators are used to ensure that CCD camera has enough exposure. In the

experiment, the test substrates are coated with hydrophobic and hydrophilic materials respectively. Ambient conditions are controlled by the control unit throughout the whole evaporation process.

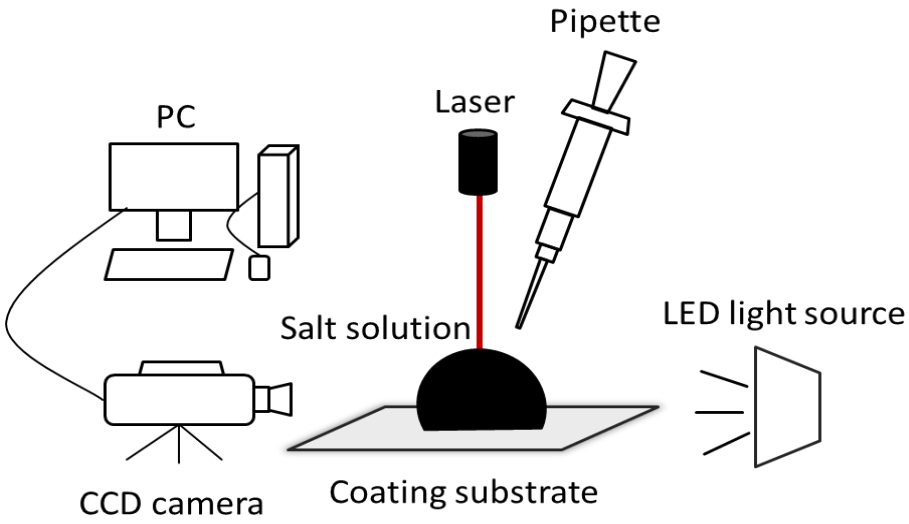

Fig.3 Experimental set-up for deposition patterns of saline droplet with both local and substrate heating on different wettability.

4 Results and Discussions

4.1 Evaporation modes and deposit patterns with different heating and wettability

Evaporation process has been investigated on both hydrophilic and hydrophilic surfaces. Generally, saline droplet evaporation process with different wettability can be divided into different modes, constant contact radius (CCR) mode, constant contact angle (CCA) mode and mixed mode, which transiting from CCR mode to CCA mode. CCR mode is an extreme case that a drop evaporating with the fixed contact line over the lifetime. Simultaneously, contact angle decreases in order to adapt to the volume loss. For CCR stage, it is an ideal condition that contact line recedes with the constant contact angle. In terms of mixed mode, it is closer to the actual condition, a drop start to evaporate with CCR mode where the contact line is pinned, contact angle simultaneously decreases until it reaches receding contact angle, at which point the contact line begins to slide. As shown in Fig.4, saline droplets are experimentally investigated with different

wettability and heating directions respectively. All the progressions are standardized to its relative time, T/T_0, where T_0 is the time for complete evaporation, T is current evaporation time. All experimental results in four groups ((a), (b), (c), (d)) show that CCR stage occupies most of the time, of which T/T_0 is at around 0.8. This ratio is beneficial for the saline solvent to transport to the edge.

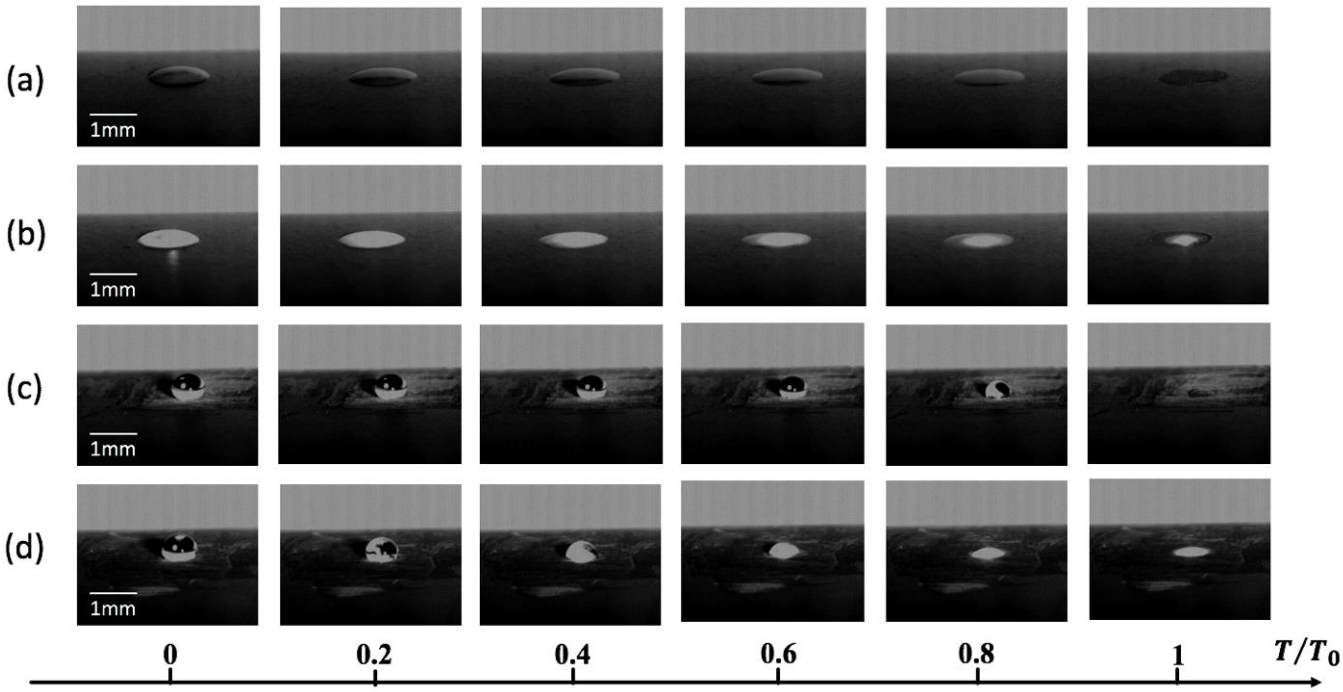

Fig.4 Record for evaporation process from substrate heating to localized heating on both hydrophilic and hydrophobic surfaces. (a) 2μL saline droplet evaporation process heated from substrate on hydrophilic surface; (b) 2μL saline droplet evaporation process heated from apex on hydrophilic surface; (c) 2μL saline droplet evaporation process heated from substrate on hydrophobic surface; (d) 2μL saline droplet evaporation process heated from apex on hydrophilic surface.

Fig.4 (a) and (b) compare the effect of both local heating from apex and substrate heating on the distribution of the saline deposition patterns with same hydrophilic surface. In the experimental results of (a) and (b), the substrate heating shows a typical ring-like structure as shown in Fig.5 (a). When it comes to local heating from apex, ring-like structure still exists, but the amount is reduced. In addition, a clear dot-like pattern appears at the heating point of droplet centre as shown in Fig.5 (b).

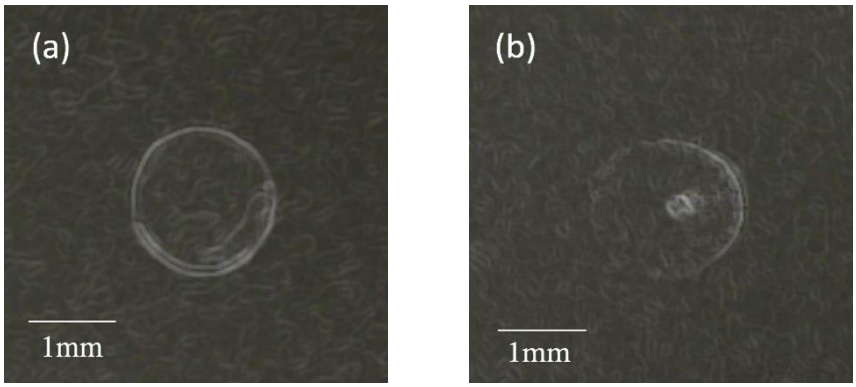

Fig.5 Substrate and local heating of saline deposition patterns on hydrophilic surface.

In terms of hydrophobic surface, different heating directions are still investigated from apex and substrate with some wettability. Compared to hydrophilic group, the deposition patterns of substrate heating show nearly the same results, most saline particles assemble along the contact line as shown in Fig.6 (a). When it comes to the localized heating from apex, different wettability shows different distributions. For hydrophilic surface, most saline particles transport from contact line to central area, forming dot-like deposition pattern, but barely saline particles are deposited between the edges and the central region as shown in Fig.5 (b). On hydrophobic surface, particles at the edge also tend to cumulate at central area. However, many deposits around between boundary and centre, which makes deposition pattern more uniform as Fig.6 (b).

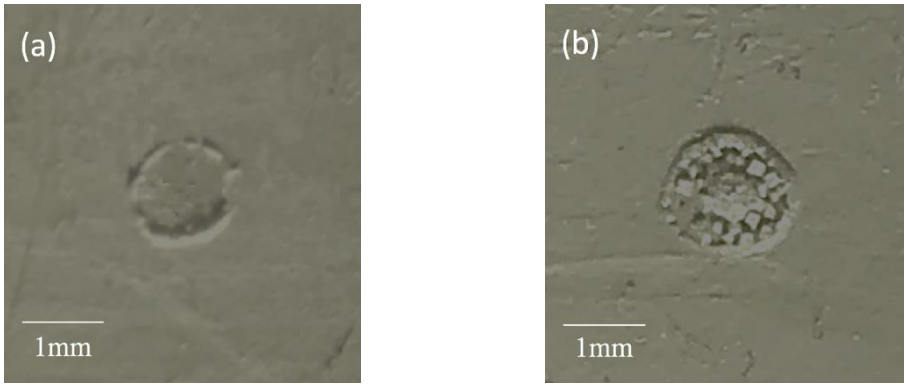

Fig.6 Substrate and local heating of saline deposition patterns on hydrophobic surface.

4.2 Mechanism of substrate heating and local heating with different wettability

For substrate heating, the temperature distribution along air-liquid interface of the saline droplet at 25°C was experimentally measured as shown in Fig.7 The experimental results show that there is a evident temperature gradient between apex and the edge along the liquid-air interface throughout evaporating process. Along droplet surface, the apex of droplet is always the coolest temperature point, while surface temperature along contact line is the highest temperature point, which leads to more solvent losing at the saline droplet boundary than that at centre. Meanwhile, CCR mode occupies most of the evaporation process, of which T/T_0 is at around 0.8. Therefore, the boundary of the saline droplet is fixed on the contact line, which means the saline solvent must flow from droplet centre toward to the edge to compensate losing solute along the contact line.

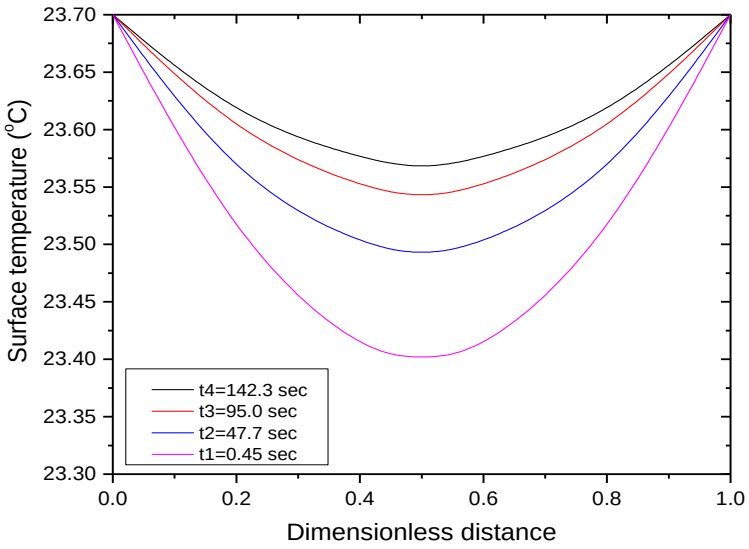

Fig.7 Surface temperature distribution profiles at 25°C.

When drying completely, most solvent has already been transported and deposited along the contact line, forming a ring-like deposition pattern shown in Fig.8 (a). Meanwhile, in this migration process, rush hour behaviour also makes a great contribution based on mass balance. The evaporation from the saline surface trigger the internal flow, meanwhile, saline evaporation flow rate remains approximately constant over the evaporation process. Since the boundary needs

to be replenished from the centre constantly, a steady flow towards to the droplet boundary is generated in the droplet. Moreover, the height of saline droplet is decreasing due to constant volume loss during evaporation process, which can be characterized by a contact angle. Therefore, same amount of solvent has to be squeezed through an area which is vanishing, inducing a diverging radial velocity. Rush hour behaviour is also regarded as having greatly contributed to coffee ring effect. It should be noticed that different wettability was little affected by the surface wettability under substrate heating. This is because temperature difference along solid-liquid interface dominates saline flow motion radially, which transport solvent from central bottom to the boundary for compensation. In this process, although wettability can affect flow along air-liquid interface, but weak. The flow motion of air-liquid interface is mainly influenced by capillary flow passively.

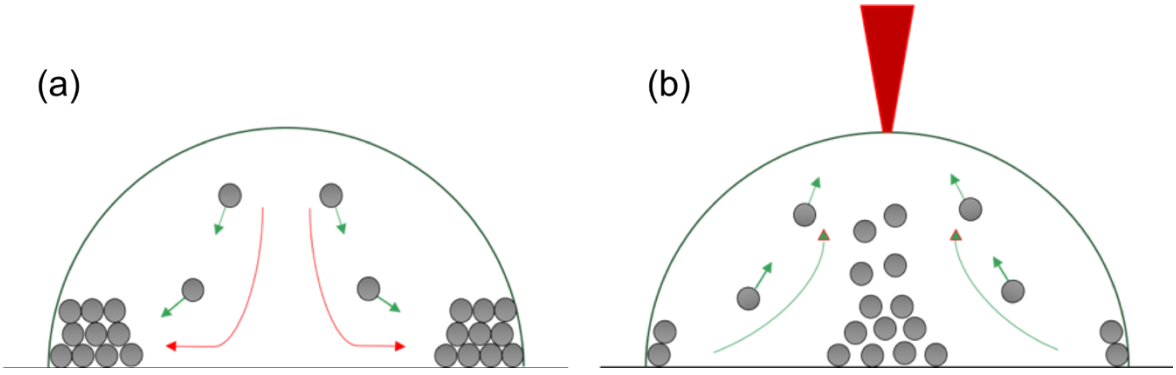

Fig.8 Schematic diagram for the mechanism of coffee ring effect and reversing internal flow by localized heating.

When it comes to localized heating, even though there is an evident temperature difference along liquid-air interface at 25°C, the local heating allows the apex of saline droplet to absorb the more energy. Therefore, surface temperature distribution is most likely opposite, which means temperature along the edge becomes the coolest, while apex is the highest temperature point. Such temperature difference results in more solvent losing at the apex than other position. More solvent must flow from periphery to apex to compensate losing solute at apex as Fig.8 (b). Therefore, most

178 solvent are hanging around apex area through the evaporation process. With droplet height
179 decreasing, hanging particles drop down gradually and most salts gathered at central area, forming
180 a dot-like pattern. Eventually, changes in surface temperature gradients lead to the changes of
181 internal flow. Compare to the substrate heating in different temperature ranges conducted by other
182 researchers[30, 31], which generally transit deposition patterns from ring-like structure to dual ring
183 and uniform, local heating and substrate heating both attempt to control the distribution of droplet
184 deposition patterns by balancing Marangoni flow and capillary flow. However, local heating
185 shows potential to actively control the distribution of deposit patterns than that of substrate heating,
186 which exhibits more potential for applications.

187 Moreover, in the case of local heating, Marangoni flow dominates flow motion of saline
188 droplet due to the temperature difference along air-liquid interface. Therefore, even though Deegan
189 et al. [32]observed that Marangoni flow, fundamentally influencing by surface tension, is weak for
190 water based droplet, that does not mean factors affecting surface tension need to be ignored in the
191 case of local heating. Wettability, as one significant factor affecting surface tension, also need to
192 be considered. Meanwhile, surface tension is the tendency of fluid surfaces to shrink into the
193 minimum surface which makes droplet tends to be spherical. Therefore, the surface area of saline
194 droplet of hydrophobic one is bigger than that of hydrophilic one. The surface free energy increases
195 with surface area, resulting in the increase of surface tension. On the other hand, in the field of
196 heat transfer, the surface tension gradient also results from a temperature gradient. The surface
197 tension of liquids decreases as temperature increases. When the saline droplet is heated from apex,
198 molecules flow from apex to the contact line along the air-liquid interface, which is a tendency to
199 impede the internal flow of saline droplet, to some extent, preventing the compensation for the
200 evaporation loss on the apex. In this process, wettability and local heating both make contribution

to surface tension, which is sometimes refer to as the Marangoni effect. [33] Therefore, on the hydrophobic surface, it is very likely that the surface tension overcomes the internal flow, so that some of the saline particles are finally dispersed between the edge and the centre, making the deposition pattern more uniform than that of hydrophilic one.

5 Conclusion

The distribution of droplet deposition patterns with both local and substrate heating on different wettability have been conducted. Experimental results show that evaporations start from CCR mode, then switch to CCA mode, CCR mode occupies most of the evaporation process. In substrate heating, the deposition patterns of saline on both hydrophobic and hydrophilic surface exhibit ring-like structure along contact line. This mainly because of the compensation for the evaporation losses along contact line due to temperature gradient along air-liquid surface. For local heating, ring-like structure switches to dot-like pattern by reversing internal flow. While for hydrophilic surface, Marangoni effect also needs to be considered. To some extent, the surface tension can balance the internal flow induced by localized heating from apex even in water-based solution. This work not only shows the potential for suppress internal flow, but also the opportunity for making deposition pattern more uniform.

Acknowledge

We acknowledge the funding EU ThermaSMART project H2020-MSCA-RISE (778104) Smart thermal management of high power microprocessors using phase-change (ThermaSMART), and from the China Scholarship Council (CSC).

References

[1] Qazi MJ, Liefferink RW, Schlegel SJ, Backus EH, Bonn D, Shahidzadeh N. Influence of surfactants on sodium chloride crystallization in confinement. *Langmuir*, 2017. **33**(17): p. 4260-4268.

[2] Melocchi A, Parietti F, Maroni A, Foppoli A, Gazzaniga A, Zema L. Hot-melt extruded filaments based on pharmaceutical grade polymers for 3D printing by fused deposition modeling. *International journal of pharmaceutics*, 2016. **509**(1-2): p. 255-263.

[3] Wei X, Yang J, Li Z, Su Y, Wang D. Comparison investigation of the effects of ionic surfactants on the crystallization behavior of calcium oxalate: From cationic to anionic surfactant. *Colloids and Surfaces A: Physicochemical and Engineering Aspects*, 2012. **401**: p. 107-115.

[4] Cole IS, Paterson DA, Ganther WD. Holistic model for atmospheric corrosion Part 6–From wet aerosol to salt deposit. *Corrosion engineering, science and technology*, 2004. **39**(3): p. 209-218.

[5] Soltman D, Subramanian V. Inkjet-printed line morphologies and temperature control of the coffee ring effect. *Langmuir*, 2008. **24**(5): p. 2224-2231.

[6] Singh M, Haverinen HM, Dhagat P, Jabbour GE. Inkjet printing—process and its applications. *Advanced materials*, 2010. **22**(6): p. 673-685.

[7] Teichler A, Perelaer J, Schubert US. Inkjet printing of organic electronics–comparison of deposition techniques and state-of-the-art developments. *Journal of Materials Chemistry C*, 2013. **1**(10): p. 1910-1925.

[8] Ramaswamy S, Golub TR. DNA microarrays in clinical oncology. *Journal of clinical oncology*, 2002. **20**(7): p. 1932-1941.

[9] Hu H, Larson RG. Marangoni effect reverses coffee-ring depositions. *The Journal of Physical Chemistry B*, 2006. **110**(14): p. 7090-7094.

[10] Colina M, Serra P, Fernández-Pradas JM, Sevilla L, Morenza JL. DNA deposition through laser induced forward transfer. *Biosensors and Bioelectronics*, 2005. **20**(8): p. 1638-1642.

[11] Deegan RD. Pattern formation in drying drops. *Physical review E*, 2000. **61**(1): p. 475.

[12] Sefiane K. Patterns from drying drops. *Advances in colloid and interface science*, 2014. **206**: p. 372-381.

[13] Zhong X, Crivoi A, Duan F. Sessile nanofluid droplet drying. *Advances in colloid and interface science*, 2015. **217**: p. 13-30.

[14] Shi L, Hu Y, He Y. Magneto-responsive thermal switch for remote-controlled locomotion and heat transfer based on magnetic nanofluid. *Nano Energy*, 2020: p. 104582.

[15] Shi L, Hu Y, Bai Y, He Y. Dynamic tuning of magnetic phase change composites for solar-thermal conversion and energy storage. *Applied Energy*, 2020. **263**: p. 114570.

[16] Brutin D, Starov V. Recent advances in droplet wetting and evaporation. *Chemical Society Reviews*, 2018. **47**(2): p. 558-585.
[17] Deegan RD, Bakajin O, Dupont TF, Huber G, Nagel SR, Witten TA. Capillary flow as the cause of ring stains from dried liquid drops. *Nature*, 1997. **389**(6653): p. 827.
[18] Majumder M, Rendall CS, Eukel JA, Wang JY, Behabtu N, Pint CL, Liu TY, Orbaek AW, Mirri F, Nam J, Barron AR. Overcoming the "coffee-stain" effect by compositional Marangoni-flow-assisted drop-drying. *The Journal of Physical Chemistry B*, 2012. **116**(22): p. 6536-6542.
[19] Askounis A, Takata Y, Sefiane K, Koutsos V, Shanahan ME. "Biodrop" Evaporation and Ring-Stain Deposits: The Significance of DNA Length. *Langmuir*, 2016. **32**(17): p. 4361-4369.
[20] Chen X, Ma R, Li J, Hao C, Guo W, Luk BL, Li SC, Yao S, Wang Z. Evaporation of droplets on superhydrophobic surfaces: Surface roughness and small droplet size effects. *Physical review letters*, 2012. **109**(11): p. 116101.
[21] Still T, Yunker PJ, Yodh AG. Surfactant-induced Marangoni eddies alter the coffee-rings of evaporating colloidal drops. *Langmuir*, 2012. **28**(11): p. 4984-4988.
[22] Kim H, Boulogne F, Um E, Jacobi I, Button E, Stone HA. Controlled uniform coating from the interplay of Marangoni flows and surface-adsorbed macromolecules. *Physical review letters*, 2016. **116**(12): p. 124501.
[23] Dague E, Jauvert E, Laplatine L, Viallet B, Thibault C, Ressier L. Assembly of live micro-organisms on microstructured PDMS stamps by convective/capillary deposition for AFM bio-experiments. *Nanotechnology*, 2011. **22**(39): p. 395102.
[24] Chhasatia VH, Joshi AS, Sun Y. Effect of relative humidity on contact angle and particle deposition morphology of an evaporating colloidal drop. *Applied Physics Letters*, 2010. **97**(23): p. 231909.
[25] Zhang M, Feng S, Wang L, Zheng Y. Lotus effect in wetting and self-cleaning. *Biotribology*, 2016. **5**: p. 31-43.
[26] Liu K, Jiang L. Bio-inspired self-cleaning surfaces. *Annual Review of Materials Research*, 2012. **42**: p. 231-263.
[27] Taylor RA, Phelan PE, Otanicar T, Adrian RJ, Prasher RS. Vapor generation in a nanoparticle liquid suspension using a focused, continuous laser. *Applied Physics Letters*, 2009. **95**(16): p. 161907.
[28] Abareshi M, Goharshadi EK, Zebarjad SM, Fadafan HK, Youssefi A. Fabrication, characterization and measurement of thermal conductivity of Fe3O4 nanofluids. *Journal of Magnetism and Magnetic Materials*, 2010. **322**(24): p. 3895-3901.
[29] Liu Z, Yan Y, Fu R, Alsaady M. Enhancement of solar energy collection with magnetic nanofluids. *Thermal Science and Engineering Progress*, 2018. **8**: p. 130-135.
[30] Li Y, Lv C, Li Z, Quéré D, Zheng Q. From coffee rings to coffee eyes. Soft Matter, 2015. **11**(23): p. 4669-4673.

[31] Parsa M, Harmand S, Sefiane K, Bigerelle M, Deltombe R. Effect of substrate temperature on pattern formation of nanoparticles from volatile drops. *Langmuir*, 2015. **31**(11): p. 3354-3367.
[32] Deegan RD, Bakajin O, Dupont TF, Huber G, Nagel SR, Witten TA. Contact line deposits in an evaporating drop. *Physical review E*, 2000. **62**(1): p. 756.
[33] McGrew JL, Bamford FL, Rehm TR. Marangoni flow: an additional mechanism in boiling heat transfer. *Science*, 1966. **153**(3740): p. 1106-1107.